Determining the Membrane Topology of Proteins: Insertion Pathway of a Transmembrane Helix of Annexin 12

Alexey S. Ladokhin,* J. Mario Isas, Harry T. Haigler, and Stephen H. White

Department of Physiology and Biophysics, University of California, Irvine, California 92697-4560

Received July 11, 2002; Revised Manuscript Received September 16, 2002

ABSTRACT: We describe a sensitive method for determining the bilayer topology of single-site cysteine-linked NBD fluorescent labels on membrane proteins. Based upon a method developed for peptides [W. C. Wimley and S. H. White (2000) *Biochemistry 39*, 161−170], it utilizes a novel fluorescence quencher, lysoUB, comprised of a single acyl chain attached to a UniBlue chromophore. The enhanced sensitivity of the method arises from the brightness of the NBD fluorescence and the quenching efficiency of lysoUB, which is not fluorescent. In the course of validating the method, we examined the insertion topology of the D−E helical region of repeat 2 of annexin 12, known to adopt a transbilayer orientation at mildly acidic pH [Langen et al. (1998) *Proc. Natl. Acad. Sci. USA 95*, 14060−14065]. In the final membrane-inserted state, an NBD label attached to the single-cysteine mutant D134C was found to be in the outer (*cis*) leaflet, while the one attached to D162C was found in the *trans* leaflet. But kinetic measurements of NBD fluorescence suggested the existence of a transient intermediate insertion state whose lifetime could be increased by increasing the fraction of anionic lipids in the vesicles. Indeed, the lifetime could be increased for times sufficient for the completion of lysoUB−NBD topology measurements. Such measurements revealed that the D−E region adopts an interfacial topology in the intermediate state with both ends on the cis side of the membrane, consistent with the general concept of interface-directed membrane insertion of proteins [White et al. (2001) *J. Biol. Chem. 276*, 32395−32398].

Determination of the topology of a particular site on a membrane protein is an important step in elucidating its structure. And even if the structure of a membrane protein is known, topology measurements are useful for verifying its correct fold and orientation after reconstitution into model membrane systems. Measurements of topology have been especially important in the determination of membrane-insertion pathways for a variety of spontaneously inserting nonconstitutive proteins, such as bacterial toxins (*1*−*3*), colicins (*4*−*7*), and annexins (*8*, *9*). Here we describe an improved method of topology determination and apply it to annexin 12.

Spectroscopic determinations of topology generally require the creation of an asymmetric (single-leaflet) bilayer distribution of an optical probe, typically a fluorescence quencher. The topology of the labeled site on the protein can then be deduced by comparing the spectroscopic response of this asymmetric distribution with the response obtained with a symmetric one (quencher in both leaflets). Such measurements can be made using quenchers attached to a double-chain lipid (*10*, *11*). But creating an asymmetric distribution is difficult and requires the use of either a special lipid exchange enzyme (*10*) or an organic solvent (*11*). The latter method is usually used only for membrane-active peptides, because organic solvents can denature proteins. Even then, moderate additions of organic solvent can destabilize the structure of the bilayer, increase spontaneous flip-flop, and consequently dissipate the asymmetric distribution of quenchers.

To avoid these problems, Wimley and White (*12*) developed a method that utilized a quencher attached to a single-chain lipid, LysoMC, which is capable of quenching tryptophan fluorescence via nonradiative Förster-type resonance energy transfer (FRET). Because single-chain lysolipids have significant water solubility and form micelles, they can be incorporated easily into the outer bilayer leaflet when added to preformed bilayer vesicles. The bulky charged quencher headgroup and single-acyl chain act in concert to slow lipid flip-flop significantly. As a result, an asymmetric distribution of LysoMC was found to be stable for times longer than necessary for topology measurements (*12*).

This method has been particularly useful for determining the topology of tryptophan-containing peptides (*13*). However, several problems arise when it is applied to proteins. First, studies with proteins necessarily involve lower concentrations of tryptophan fluorophore than peptide studies, because there is at least an order-of-magnitude decrease in concentration (assuming one tryptophan per one polypeptide chain). Tryptophan, which serves as a donor for the LysoMC FRET method, is not bright enough under these circumstances. Second, measuring tryptophan fluorescence in proteins requires the use of a longer excitation wavelength

* To whom correspondence should be addressed. Phone: 949-824-6993. FAX: 949-824-8540. E-mail: ladokhin@uci.edu. Permanent address: Institute of Molecular Biology and Genetics, National Academy of Sciences of Ukraine, Kiev 252143, Ukraine.

† This research was supported in part by grants from the National Institute of General Medical Science (GM-46823 and GM-55651).

10.1021/bi0264418 CCC: $22.00
Published on Web 10/26/2002

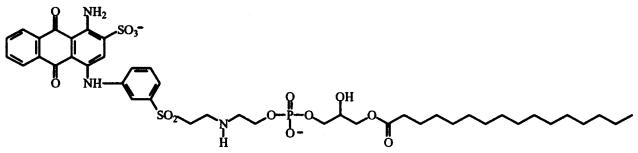

FIGURE 1: Chemical structure of lysoUB, a novel compound consisting of a UniBlue A chromophore attached to a lysolipid.

to ensure photo selection in the presence of tyrosine residues. Switching from 270 to 280 nm excitation—good for tyrosine-free peptides—to 295 nm, which is needed for proteins containing tyrosines, not only increases the scattering background but also increases the direct contribution of unproductive LysoMC fluorescence into the total emission signal.

We overcame these difficulties in the following ways in order to extend the Wimley and White (*12*) methods to proteins. First, we used an NBD chromophore that has a 5-fold higher extinction coefficient (*14*) than tryptophan, as well as a generally higher quantum yield in nonpolar environments (*15*). NBD also fluoresces at a longer wavelength than tryptophan, which reduces the contribution of membrane scattering. NBD is easily incorporated into proteins by selectively labeling cysteine side chains (*16*). Because the much smaller cysteine is more easily introduced into a specific site than bulkier tryptophan, a further advantage is gained. Second, we used a novel nonfluorescing quencher, lysoUB (Figure 1), which is a lysolipid derivative of UniBlue chromophore that quenches NBD fluorescence via nonradiative energy transfer. The lack of fluorescence from UniBlue circumvents contamination of NBD fluorescence with quencher fluorescence. Finally, we developed a single-sample differential experimental scheme that increases measurement reliability by avoiding the necessity of comparing two different samples.

After validating the method by using artificially created all-*cis* (i.e. outer leaflet only), all-*trans*, and isotropic distributions of NBD, we tested it in a protein system by studying the insertion of a transmembrane region of annexin 12. Annexins constitute a structurally conserved family of proteins implicated in a variety of membrane-related functions, including vesicular trafficking, membrane fusion, and ion-channel formation (*17*, *18*). High-resolution crystal structures of the soluble forms of several different annexins, including annexin 12 (*19*), reveal a common fold. Besides the well-documented Ca^{2+}-dependent binding of annexins to membrane interfaces (*20*), a recent site-directed spin labeling study has demonstrated pH-induced transmembrane insertion of annexin 12 (*8*). Under mildly acidic conditions (pH 4−5), the D−E region of the second repeat undergoes a transition from a helix−loop−helix conformation in the soluble form to a transmembrane helix in the inserted form. The orientation of the inserted helix, however, was not determined. To determine its orientation, we used single-cysteine mutants (D134C and D162C) flanking the proposed transmembrane region and studied their insertion into various lipid systems. Our results revealed that the D−E region passed through an interfacial intermediate state prior to final insertion of the N-terminus of the helix across the bilayer and that the interfacial intermediate could be stabilized by increasing the concentration of anionic lipids. A preliminary account of this work has appeared elsewhere (*21*).

MATERIALS AND METHODS

Materials. POPC,[1] POPG, PC (a mixture of phosphatidylcholine lipids from egg yolk, catalog no. 840051), PS (a mixture of phosphatidylserine lipids from bovine brain, catalog no. 84032), NBD-PE, and lysoPE were purchased from Avanti Polar Lipids (Alabaster, AL). UniBlue A vinyl sulfone and alamethicin were purchased from Sigma (St. Louis, MO). IANBD was purchased from Molecular Probes (Eugene, OR). Two buffers were used, acidic (100 mM sodium acetate, pH 4.5) and neutral (20 mM HEPES, 100 mM NaCl, pH 7.4).

Synthesis and Purification of LysoUB. LysoUB (Figure 1) was synthesized by covalently attaching the UniBlu A probe to the primary amino group of the lysoPE headgroup. This was accomplished by mixing 50 mg of UniBlue A vinyl sulfone, an amine-reactive reagent (*22*), in 0.5 mL of 0.2 M sodium carbonate (pH 11) with 20 mg of 1-palmitoyl-2-hydroxy-*sn*-glycero-3-phosphoethanolamine (lysoPE) in 1 mL of 2 M diisopropylethylamine in *N*-methylpyrrolidinone. The mixture was incubated overnight at room temperature, dried under a stream of N_2, and lyophilized. The lysophospholipids were separated from all the other reactants and products by means of five repeated chloroform−water extractions. The sample was resuspended in a mixture of 25 mL of water and 5 mL of chloroform, mixed vigorously, and allowed to phase-separate. The water fraction was removed and the chloroform fraction was saved for the next extraction. LysoUB was separated from lysoPE using preparative thin-layer chromatography in a solvent system consisting of 65% $CHCl_3$, 30% CH_3OH, 2.5% H_2O, and 2.5% NH_4OH. LysoPE remained near the origin ($R_f \sim 0.1$) and lysoUB migrated with $R_f \sim 0.8$. Purified lysoUB was stored in 1:1 $CHCl_3$:CH_3OH at −20 °C. Analytical thin-layer chromatography and fluorescence quenching indicate that lysoUB is chemically stable for several months. The concentration of the stock solution was determined spectrophotometrically, assuming an extinction of 11 000 $M^{-1}cm^{-1}$ at 617 nm (*14*).

NBD Labeling of Single-Cysteine Mutants of Annexin 12. Single-cysteine mutations were made at positions 134 (Asp), 144 (Ser), and 162 (Asp), and the mutants were isolated as described previously (*8*). NBD-labeling was done using a standard procedure for the thiol-reactive derivative IANBD (*14*). In a typical labeling reaction, five 1 μL aliquots of 0.4 M IANBD in DMSO were mixed with 2 mL of a 2 mg/mL sample of single-cysteine annexin mutant in a DTT-free

[1] Abbreviations: Anx134-NBD, Anx144-NBD, and Anx162-NBD, NBD labeled single-cysteine mutants D134C, S144C, and D162C of annexin 12, respectively. FRET, Förster resonance energy transfer. IANBD amide, *N*,*N*′-dimethyl-*N*-(iodoacetyl)-*N*′-(7-nitrobenz-2-oxa-1,3-diazol-4-yl)ethylenediamine. LUV, extruded large unilamellar vesicles of 100 nm diameter. LysoPE, 1-palmitoyl-2-hydroxyl-*sn*-glycero-3-phosphoethanolamine. LysoMC, *N*-(7-hydroxyl-4-methylcoumarin-3-acetyl)-1-palmitoyl-2-hydroxy-*sn*-glycero-3-phosphoethanolamine. LysoUB, UniBlue-1-palmitoyl-2-hydroxy-*sn*-glycero-3-phosphoethanolamine. NBD, 7-nitrobenz-2-oxa-1,3-diazol-4-yl. NBD-PE, *N*-(7-nitrobenz-2-oxa-1,3-diazol-4-yl)-1-palmitoyl-2-oleoyl-*sn*-glycero-3-phosphoethanolamine. POPC, palmitoyloleoylphosphatidylcholine. POPG, palmitoyloleoylphosphatidylglycerol. PC, egg yolk phosphatidylcholine. PS, bovine brain phosphatidylserine. PS/PC, a 2:1 weight ratio mixture of PS and PC. 25POPG/75POPC and 75POPG/25POPC, mixtures of POPG and POPC that contain a molar percentage of corresponding lipid specified by the number.

buffer at pH 7.4. The sample was incubated overnight at 4 °C in the dark and then passed through a PD-10 gel filtration column to remove IANBD. The extent of labeling was found to be in the range of 0.5−0.8, estimated from absorbance spectra using extinction coefficients of 25 000 $M^{-1}cm^{-1}$ for NBD at 480 nm (*14*) and 12 300 M^{-1} cm^{-1} for annexin at 278 nm.

Sample Preparation. Large unilamellar vesicles of diameter 0.1 μm were prepared by extrusion (*23*, *24*) using the following lipid mixtures: 2:1 (w:w) mixture of bovine brain phosphatidylserine and egg yolk phosphatidylcholine (PS/PC), 1:3 molar mixture of POPG and POPC (25POPG/75POPC), and 3:1 molar mixture of POPG and POPC (75POPG/25POPC). For the NBD-PE sample, 2% NBD-PE in POPC was used. Membrane insertion was induced by adding the stock solutions of proteins and LUV to 1 mL of pH 4.5 buffer to give a final concentration of 0.04 μM protein and 40 μM lipid. For topology experiments with PS/PC, 2 mL samples containing 0.01 μM protein and 10 μM lipid were used to prevent vesicle aggregation. For NBD-PE experiments, 1 mL samples of 40 μM lipid were used. Asymmetric distributions of lysoUB were created as follows: (1) Appropriate volumes (0.5−10 μL) of a stock solution of lysoUB in chloroform−methanol were dried on the bottom of a test tube; (2) a sample containing LUV and protein was then placed in the test tube and gently mixed for 5 min; (3) the sample was removed from the tube and placed in a cuvette for fluorescence measurements. Because lysoUB flip-flops at a very low rate, this procedure yields LUV with label only in the outer leaflet. Symmetric distributions of lysoUB were obtained from the asymmetric ones by adding 0.5 μL of 5 mg/mL alamethicin in methanol directly to the asymmetric samples. This amount of alamethicin was sufficient to cause flip-flop remixing of lipids within 10 min (*12*). For Ca^{2+}-dependent binding of Anx144-NBD, membrane interactions were initiated by adding 1 mM Ca^{2+} at pH 7.4 to the sample containing 40 μM of lipid and 0.08 μM of protein.

An all-trans distribution of NBD-PE was prepared by adding 10 μL of freshly made 1 M sodium dithionite to a 0.5 mL sample containing 1 mM POPC with isotropically distributed NBD-PE. After 10 min of incubation, when the outer layer NBD was chemically modified (*25*), the excess sodium dithionite was removed on a PD-10 gel filtration column. A second addition of dithionite to the sample did not result in any reduction of NBD fluorescence, indicating that the remaining fluorescence originates from the fluorophores located in the inner leaflet. The sample with this asymmetric distribution of NBD-PE was used within a few hours of preparation, although it appeared stable for several days.

Fluorescence. Fluorescence was measured using an SLM 8100 steady-state fluorescence spectrometer (Jobin Yvon, Edison, NJ) equipped with double-grating excitation and single-grating emission monochromators. The measurements were made in 4 × 10 mm or 10 × 10 mm cuvettes, thermostated to 25 °C. Cross-orientation of polarizers was used (excitation polarization set to horizontal, emission polarization set to vertical) in order to minimize the scattering contribution from vesicles and to eliminate spectral polarization effects in monochromator transmittance (*26*). NBD fluorescence spectra were obtained by averaging 3−20 scans collected over a 480−600 nm range using 1 nm steps. The excitation wavelength was 470 nm. Excitation slits were no larger than 4 nm and emission slits were no larger than 8 nm. The background spectra did not contain any signals other than Raman and Raleigh scattering and were not subtracted from the spectra collected from NBD-containing samples. During fluorescence kinetics measurements, the entrance slit on the excitation monochromator was reduced to 1 nm to minimize photobleaching during the measurement. The intensity of control samples of NBD-PE or NBD-labeled annexins remained unchanged for many hours under these conditions. During kinetic measurements the emission monochromator was set to 530 nm and the slits to 16 nm.

Resonance Energy Transfer. The energy transfer efficiency E depends on the distance r between donor (NBD) and acceptor (lysoUB) and the Förster distance R_0:

$$E = R_0^6/(R_0^6 + r^6) \quad (1)$$

The Förster distance is generally computed from (*27*)

$$R_0 = 9.79 \times 10^3(\kappa^2 n^{-4} \phi_d J)^{1/6}\ (\text{Å}) \quad (2)$$

where κ^2 describes the relative orientations of acceptor and donor, n is the refractive index of the medium, ϕ_d the quantum yield of the donor, and J the integral of the spectral overlap between the donor emission and the acceptor absorption. If the donor and acceptor are isotropically oriented, as frequently assumed, then $\kappa^2 = 2/3$. The assumptions related to the application of the energy transfer method in membrane systems and to calculations of R_0 have been addressed in the literature (*12*, *28*−*30*). In the method outlined here, however, the precise value of R_0 does not matter. Assuming ϕ_d can range from 0.3 to 0.75 (*15*) and given all the potential uncertainties in other parameters (discussed in detail by Wimley and White (*12*)), we have estimated R_0 for the NBD-lysoUB donor−acceptor pair in a membrane environment to be between 33 and 38 Å, approximately equal to hydrocarbon-core thickness of the bilayer. As a result, quenching within the same leaflet is much more efficient than trans-leaflet quenching, as shown by studies with model systems (see Results).

Single-Sample Differential Experimental Scheme for Topology Determination. To avoid the use of double samples used in the original Wimley and White (*12*) method, we developed a single-sample differential scheme for determination of the membrane topology using NBD/lysoUB quenching. In Figure 2, three cases are considered: all-*cis* NBD location (A), all-*trans* NBD location (B), and isotropic *cis*/*trans* distribution (C). When added to the preformed lipid bilayers, lysolipids will first incorporate into the outer leaflet. Because the headgroup of the chromophore is bulky and charged, its spontaneous flip-flop into the inner leaflet is not efficient (*12*). Consequently, stable asymmetric distributions with lysoUB localized in the outer leaflet (Figure 2, left-hand panels) can be prepared. This distribution can be transformed into a symmetric one with a uniform distribution of lysoUB in both leaflets (Figure 2, right-hand panels) by adding a lipid flip-flop-inducing agent, such as alamethicin. Thus, in a single-sample differential scheme, fluorescence of the same sample in the same cuvette is measured before and after the addition of alamethicin. This constitutes a key

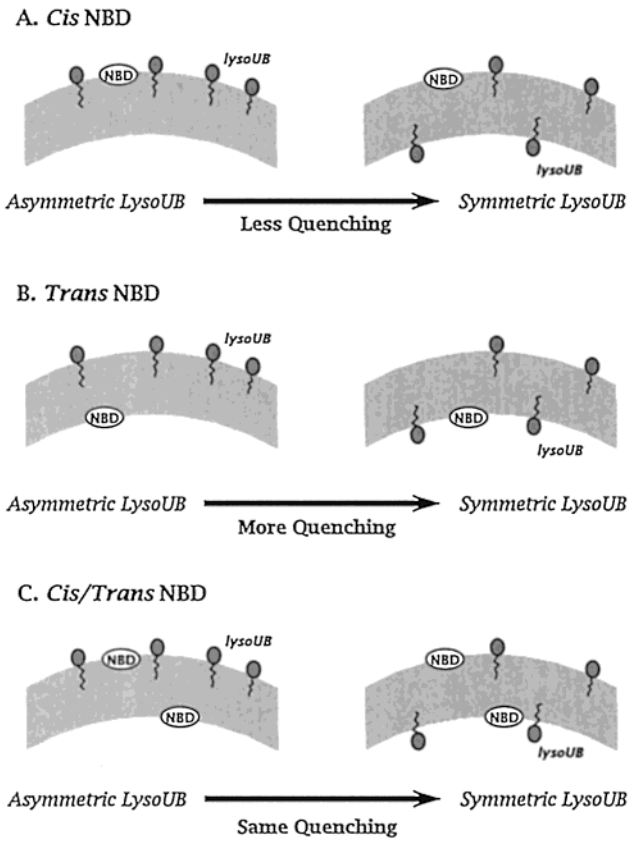

FIGURE 2: Schematic representation of a single-sample experimental scheme for determining membrane topology of the NBD-labeled protein. LysoUB quencher can be incorporated into the outer leaflet, resulting in asymmetric distribution (left-hand panels), which subsequently can be transformed into a symmetric distribution (right-hand panels) by adding a lipid flip-flop-inducing agent such as alamethicin. Because lysoUB quenching is stronger for NBD located in the same leaflet, this transformation (represented by arrows) will change the amount of quenching in the following ways: (A) for all *cis*-NBD the quenching decreases, because half of the lysoUB is transferred into the opposite leaflet; (B) for *all-trans*-NBD the quenching increases, because half of the lysoUB is transferred into the same leaflet; (C) for an equimolar mixture of *cis*- and *trans*-NBD the quenching remains approximately the same, because the two processes tend to cancel each other. This experimental scheme increases the reliability of measurements by avoiding the need to compare two separately prepared samples, one with symmetric and one with asymmetric distribution of quenchers.

difference between the proposed scheme and the conventional two-sample scheme (*12*), in which symmetric and asymmetric distributions are formed separately and fluorescence signals of the two samples are compared. The use of a single sample reduces the variations caused by sample preparation, which could be quite significant given the nature of membrane protein samples.

Because lysoUB quenching is stronger for NBD located in the same leaflet, the transformation to a symmetric distribution (represented by arrows in Figure 2) will change the amount of quenching, depending on the NBD topology. For *all-cis*-NBD (Figure 2A) this will lead to depletion of efficient quenchers, because half of the lysoUB is transferred into the opposite leaflet. The resulting quenching is expected to decrease (increased intensity). For *all-trans*-NBD (Figure 2B), the opposite should be true, and more quenching (lower intensity) is expected upon the conversion from asymmetric to symmetric distribution of NBD. For an equimolar mixture of *cis*- and *trans*-NBD (Figure 2C), the quenching remains approximately the same, because the two processes tend to cancel each other. To be absolutely accurate, in the latter case a slight decrease of intensity is expected, because the concentration dependence of quenching is not a linear function (*28*). It follows from these general considerations that measurements of intensity changes following the conversion of vesicles from asymmetric to symmetric lysoUB distributions will provide information on the topology of the NBD probe.

Kinetic Simulations. The time course of the fluorescence intensity change, *F(t)*, along a W (water-soluble) ↔ I (interfacial intermediate) ↔ T (transmembrane) pathway was simulated using

$$F(t) = F_W f_W(t) + F_I f_I(t) + F_T f_T(t) \quad (3)$$

where F_W, F_I, and F_T are the intensities and f_W, f_I, and f_T are the fractional populations of the W, I, and T states, respectively. The time dependencies of the fractional populations are given by (*31*)

$$f_W(t) = e^{-k_1 t} \quad (4a)$$

$$f_I(t) = \frac{k_1}{k_2 - k_1}(e^{-k_1 t} - e^{-k_2 t}) \quad (4b)$$

$$f_T(t) = 1 - f_W(t) - f_I(t) \quad (4c)$$

where k_1 is the rate of the W → I transition and k_2 the rate of the I → T transition. The underlying assumption is that the reverse rates can be neglected compared to the direct rates, i.e. rate for the W ← I and I ← T transition is much smaller than that for the W → I and I → T transition, respectively. This assumption significantly simplifies the mathematical expression of the kinetics, which is used only for the purpose of illustration. Two limiting cases were considered: (1) the second step is rate-limiting, $k_1 = 3 \times 10^{-3}$ s^{-1} and $k_2 = 3 \times 10^{-5}$ s^{-1}, and (2) both steps have similar rates, $k_1 = 3 \times 10^{-3}$ s^{-1} and $k_2 = 2.7 \times 10^{-3}$ s^{-1}. The same set of intensity values was used in both cases: $F_W = 1.5$, $F_I = 8.5$, and $F_T = 5.5$

RESULTS

LysoUB Quenching of NBD Fluorescence. Figure 3A shows that the absorbance spectrum of lysoUB (dashed curve) and the fluorescence spectrum of NBD-PE in POPC LUV (solid line) overlap significantly, thus providing the conditions for effective Förster-type resonance energy transfer (FRET) quenching in the membrane environment. Titration with lysoUB of NDB-PE-containing POPC LUV shows strong, progressive quenching of the NBD (Figure 3B). The Förster radius of transfer, R_0, estimated from the overlap integral of absorbance and emission under standard assumptions, was found to be about 35 Å, which is about the same as the thickness of the bilayer hydrocarbon core (see Materials and Methods). The efficiency of transfer thus differs for donor and acceptor distributed in the same or in opposite leaflets. This provides the conditions necessary for the single-sample differential experimental scheme for topol-

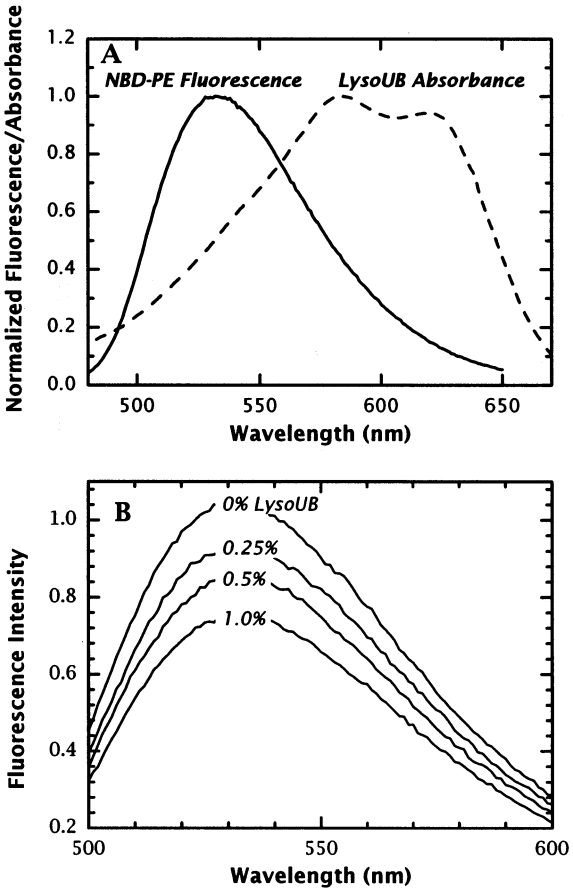

FIGURE 3: (A) The absorbance spectrum of lysoUB (dashed curve) overlaps with a typical NBD fluorescence spectrum in a lipid environment (NBD-PE in POPC, solid line), providing conditions for effective quenching via Förster-type resonance energy transfer (FRET) in the membrane environment. (B) Progressive quenching of fluorescence of NBD-PE in POPC vesicles is observed upon titration with lysoUB.

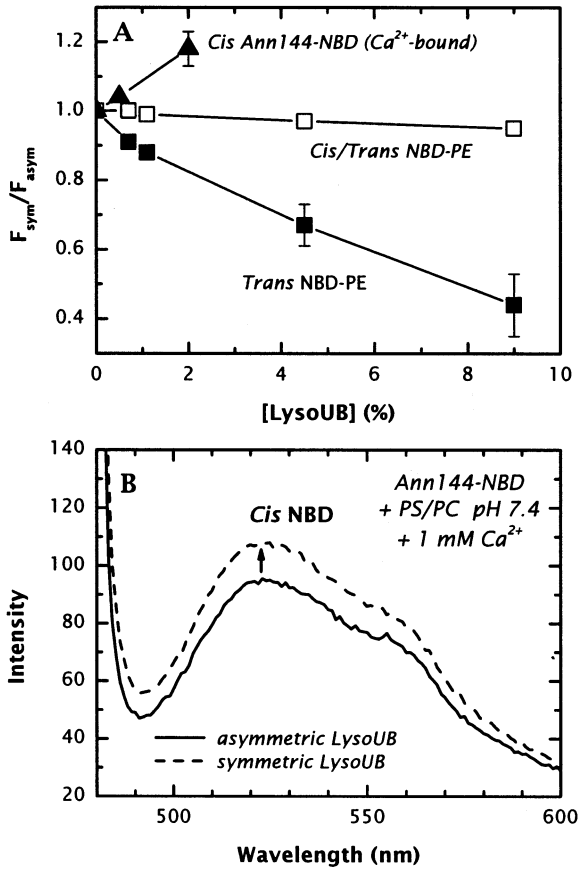

FIGURE 4: (A) Tests of the lysoUB topology method with three model systems emulating the three cases in Figure 2. The ratio of fluorescence intensities at 530 nm measured with a symmetrical distribution of lysoUB (F_{sym}) and with an asymmetrical distribution of lysoUB (F_{asym}) is plotted against the quencher concentration expressed as a percentage of the total lipid. The *cis* distribution of NBD was modeled by an NBD-labeled single-cysteine mutant of annexin 12 bound interfacially at neutral pH in a Ca^{2+}-dependent mode (▲). The *cis*/*trans* distribution was modeled by vesicles formed of 2% NBD-PE in POPC (□). The *trans* distribution was modeled with the same vesicles after the NBD fluorophores in the outer layer were chemically modified with sodium dithionite (■). In all three cases, the fluorescence changes in accordance with the scheme from Figure 2. The error bars show the standard deviations of experiments performed in triplicate. (B) Tests of the lysoUB topology method with NBD-labeled annexin interfacially bound to PS/PC LUV at pH 7.4 in the presence of 1 mM Ca^{2+}. Ca^{2+}-dependent binding results in peripheral association of the folded protein with the same structural fold as observed in the X-ray crystal structure (*32*). This system thus corresponds to the case of an all-*cis* location of NBD (Figure 2A). After mixing 40 μM PS/PC LUV and 0.08 μM Anx-144NBD, 2% lysoUB was introduced into the outer leaflet, and fluorescence corresponding to this asymmetric distribution was measured (solid line). Then a symmetric distribution of lysoUB was created in the same sample after addition of alamethicin, which causes lipid flip-flop (*12*). The fluorescence intensity of the spectrum collected with this symmetric distribution (dotted line) is higher, consistent with the prediction of Figure 2A. The sample used in this experiment contained twice the amount of protein compared to low pH samples used in our study. Therefore, the data illustrate what the expected best quality spectra and intensity changes should look like in our topology determination experiments.

ogy determination using the NBD-lysoUB donor−acceptor pair, described in Materials and Methods.

Testing the Single-Sample Differential Topology Method on Model Systems. As a first test of the general sensitivity of the method, we modeled the *trans*- and *cis/trans*-NBD topology (Figure 2B, C) using two different preparations of NBD-PE in POPC LUV. Isotropic distribution of NBD-PE in both leaflets was easily achieved by forming the LUV from a mixture of labeled and unlabeled lipid. The trans distribution (NBD inside) was obtained from the isotropic one by chemical modification of the external NBD-PE using dithionite (see Methods). Various amounts of lysoUB were then added to the two preparations, which labeled the outer leaflet of each preparation. The fluorescence intensity, F_{asym}, was measured. We then added alamethicin to cause a flip-flop of lysoUB, in order to change the distribution of lysoUB to a symmetric one, and measured the fluorescence, F_{sym}. The ratio of F_{sym}/F_{asym} is plotted against the concentration of lysoUB expressed as a percentage of the total lipid in Figure 4A (square symbols). In both cases the intensity changes followed the trends predicted in Figure 2: as the lysoUB concentration increased, F_{sym}/F_{asym} remained constant in the cis/trans sample (Figure 4A, open squares) but decreased in the trans sample (Figure 4A, closed squares). Of course, the addition of alamethicin to the all-trans distribution of NBD-PE should cause flip-flop of the NBD-PE as well as quencher. But this does not matter, because in both cases the intensity is expected to decrease, which is indeed observed experimentally (Figure 4A, solid squares). We concluded that the lysoUB method implemented according to the scheme in Figure 2 could indeed be used to

determine the topology of NBD-labeled sites, at least for cis/trans and all-trans distributions.

Two questions remained. First, does the method work for a labeled protein? And, second, can a cis distribution be detected? Both questions were addressed using an NBD-labeled Ser144Cys annexin 12 mutant, Anx144-NBD, bound to PS/PC LUV at neutral pH in the presence of Ca^{2+}. Previous studies established that Ca^{2+}-dependent binding of annexins to membranes results in a peripheral location of the protein, with a structure similar to that determined by crystallography (*32*−*34*). The side chain of position 144 of annexin 12 projects directly toward the bilayers, and detailed site-directed spin labeling studies of this region show that this side chain interacts directly with the interfacial region of the outer leaflet of the bilayer (M. Isas, R. Langen, W. Hubbell, and H. Haigler, unpublished results). In the current study, Anx144-NBD was mixed with the LUV and binding then was initiated by addition of 1 mM Ca^{2+}. A severalfold increase in NBD fluorescence was observed, indicting a strong interaction of the protein with the membrane surface. LysoUB (2% of total lipid) was then introduced into the outer leaflet (see Methods), and the fluorescence corresponding to this asymmetric distribution was measured (Figure 4B, solid line). Raw data, i.e., those not corrected for background, are shown in Figure 4B so that the relative contributions of NBD fluorescence and Raleigh and Raman scattering can be appreciated. We then added a small amount of an alamethicin−methanol solution to the sample. This causes lipid flip-flop (*12*) and consequently a symmetric distribution of lysoUB. Because the total amount of alamethicin used is less than 1:100 of the annexin on a gram per gram ratio, it is extremely unlikely that the addition of alamethicin changed the topology of the protein. Consistent with the prediction of Figure 2A, this induction of a symmetric lysoUB distribution resulted in an increased intensity (dashed curve, Figure 4B; triangles, Figure 4A). These results demonstrate not only that a cis-distribution of a NBD label can be detected but that it can be detected using a single NBD label on a protein. Figure 4B served as a useful visual reference frame in our subsequent studies of annexin insertion. As a control experiment, we added alamethicin in the absence of quencher, which had no effect on the fluorescence properties of NBD-labeled annexin. Thus, if there was any interaction of alamethicin with NBD-labeled annexin, it was not apparent spectroscopically.

Kinetic Measurements of Annexin 12 Binding to Membranes. We prepared two NBD-labeled single-cysteine mutants, Anx134-NBD and Anx162-NBD, to determine the topology of the D−E helical region of annexin 12. The labels were chosen so that they were located a few residues from either end of the transmembrane helical region identified by site-selective EPR measurements (*8*). However, before topology could be determined, we had to make sure that the system had reached a relatively stable state in which fluorescence did not change significantly for the duration of an experiment (about 10−20 min). Because NBD fluorescence is extremely sensitive to the polarity of the probe's environment, it provided a convenient tool for studying temporal rearrangements during insertion.

Figure 5A presents fluorescence kinetics data for the interaction of Anx162-NBD with two lipid systems carried out at pH 4.5 in the absence of Ca^{2+}, conditions known to promote transmembrane insertion of annexin 12 (*8*). Upon mixing with lipid, protein NBD fluorescence increased substantially, consistent with the transfer of water-exposed NBD to a shielded environment. The kinetic behavior of protein binding to 75POPG/25POPC was complex: the intensity reached a maximum quickly and then slowly declined. This change in fluorescence indicated the existence of an intermediate state with higher fluorescence intensity. On the other hand, such an intermediate was not apparent for the binding of Anx162-NBD to 25POPG/75POPC; the intensity leveled off reasonably quickly and stayed constant for many hours. The intensity level, however, was much lower, suggesting a different probe environment than for binding to 75POPG/25POPC.

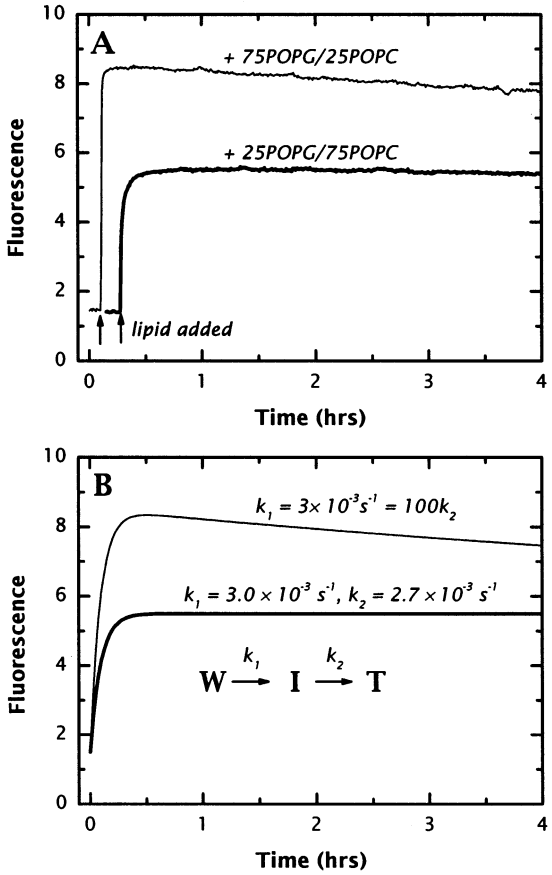

FIGURE 5: (A) Fluorescence kinetics of Anx162-NBD upon additions of lipid vesicles. Binding to 75POPG/25POPC LUV (upper curve) has a more complex biphasic kinetics than that to 25POPG/75POPC LUV (lower curve). The overall increase of fluorescence in the two-lipid systems is different, suggesting the possibility of an intermediate state with different topology (see Figures 6 and 7). (B) Simulation of the insertion pathway involving a high-intensity intermediate state (details in text). The higher curve illustrates the case when the rate of formation of the intermediate, k_1, is 100-fold higher than the rate of the final insertion, k_2. The lower curve corresponds to the case when both constants have approximately the same value.

A reasonable explanation for the results of Figure 5A is the existence of an intermediate (I) in the pathway from the water-soluble state (W) to a final state (T). It is possible that the intensities of the final and intermediate states are quite similar in the two lipid systems and that the main difference is due to varying conversion rates. To illustrate this possibility, we simulated fluorescence kinetics along a W → I → T pathway using eqs 3 and 4 (Materials and

Methods). The two curves presented in Figure 5B were generated using different values for the rate constants, k_1 for W → I and k_2 for I → T, assuming the intensities of each state were equal in the two lipid systems. For the upper curve, the two rates differ by 2 orders of magnitude ($k_1 = 3 \times 10^{-3}$ s^{-1}, $k_2 = 3 \times 10^{-5}$ s^{-1}), so that the second step is rate limiting. This causes the system to be trapped in the intermediate state. For the lower curve, the two rates are about the same ($k_1 = 3 \times 10^{-3}$ s^{-1}, $k_2 = 2.7 \times 10^{-3}$ s^{-1}). Despite the fact that the fraction of the high intensity I-state reaches almost 40% during early times (data not shown), its appearance in the fluorescence kinetics is not obvious. These simulations suggested that the concentration of POPG can affect the lifetime of the intermediate state.

But regardless of the exact nature of the kinetic changes, they are slow (hours) relative to the time required for a topology determination (minutes). This means that topology can be determined during the kinetic processes. Consequently, if the intermediate and final state have different topologies, these should be detectable by doing the measurements in different lipid systems and at different incubation times.

Topology of the D−E Helical Region of Annexin 12 in LUV. As in earlier EPR measurements (*8*), insertion of the D−E helical region of annexin 12 was initiated by mixing labeled protein with LUV at pH 4.5. Topology determinations for the two mutants in 25POPG/75POPC LUV is presented in Figure 6. After a 1-h initial incubation, 2% lysoUB was incorporated into the outer leaflet, and the fluorescence spectrum for the asymmetric distribution was measured (Figure 6, solid lines). Then alamethicin was added to induce transbilayer mixing of the distribution of the lysoUB quencher. After 20 min of incubation, the spectrum for the symmetrized lysoUB distribution was measured (Figure 6, dashed lines). The changes in fluorescence observed for the two mutants were clear and unambiguous: They were in opposite directions, consistent with different topologies. For Anx134-NBD, the increase observed (Figure 6A) indicated a cis location of the probe, while the decrease observed for the Anx162-NBD (Figure 6B) indicated a trans-location of the probe. One can reasonably conclude that the Anx162-NBD probe was translocated across the membrane at low pH, whereas the Anx134-NBD probe was not.

These experiments were repeated using 75POPG/25POPC vesicles. While Anx134-NBD bound to 75POPG/25POPC showed the same topology as in 25POPG/75POPC lipid (data not shown), the topology of Anx162-NBD was found to be different. After a 1-h incubation with 75POPG/25POPC, the probe was still found on the cis side, as shown in Figure 7A. After a 20-h incubation, only a partial translocation was observed (Figure 7B). These data suggested that the intermediate state proposed in Figure 5 is one in which the residues associated with the annexin TM helix were on the surface of the membrane. That is, the intermediate was an interfacial intermediate state on the annexin membrane-insertion pathway.

The results to this point indicated that an increase in POPG slows down the helix insertion process. To establish that the topology observed was not a peculiarity of POPG, we carried out similar experiments using the PS/PC lipid system that was used in the original spin labeling study (*8*). A 5-h incubation was necessary to reach an equilibrium state, which

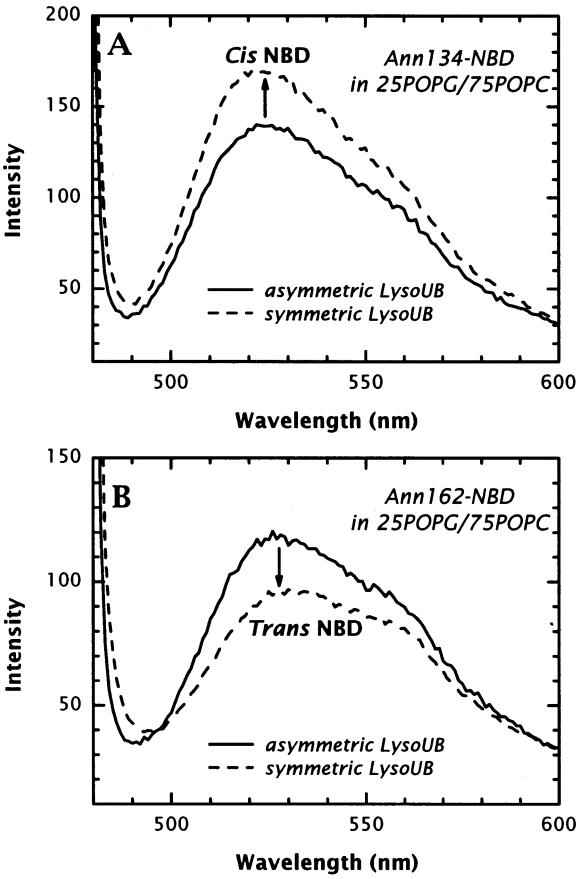

FIGURE 6: Determination of topology of the D−E helix of annexin 12 inserted into 25POPG/75POPC LUV at pH 4.5. The samples were incubated for 1 h before the measurements. First, the fluorescence of NBD-labeled single-cysteine mutants was measured in the presence of an asymmetric distribution of lysoUB (solid lines). Fluorescence was then measured after the lysoUB distribution converted into a symmetric one by adding alamethicin, which causes lipid flip-flop (dashed lines). The latter caused increase in fluorescence of a mutant labeled at position 134 (A), and decrease in fluorescence of a mutant labeled at position 162 (B). This is consistent with the *cis*- and *trans*-leaflet location for the probe in Anx134-NBD and Anx162-NBD, respectively.

is longer than for 25POPG/75POPC but shorter than for 75POPG/25POPC. A difficulty with PS/PC LUV is that they are susceptible to aggregation, especially after addition of alamethicin, which resulted in increased scattering and interfered with the assay. To combat this problem, measurements were performed at very low concentrations (0.01 μM of protein and 10 μM of lipid). Nevertheless, the result is clear (Figure 8) and is exactly the same as with 25POPG/75POPC (compare to Figure 6): the probe attached at position 162 is translocated, while the one attached at position 134 remains on the cis side of the bilayer.

DISCUSSION

We have described a robust method for determining the topology of NBD-labeled membrane proteins that utilizes a novel FRET quencher, lysoUB. Using an NBD-lysoUB pair combines the advantages of a bright donor chromophore and of a nonfluorescing acceptor. Another important advance is the introduction of a single-sample differential experimental scheme (Figure 2) in which the symmetric distribution of quenchers is assembled directly from the asymmetric one, precluding the necessity for a separate sample preparation

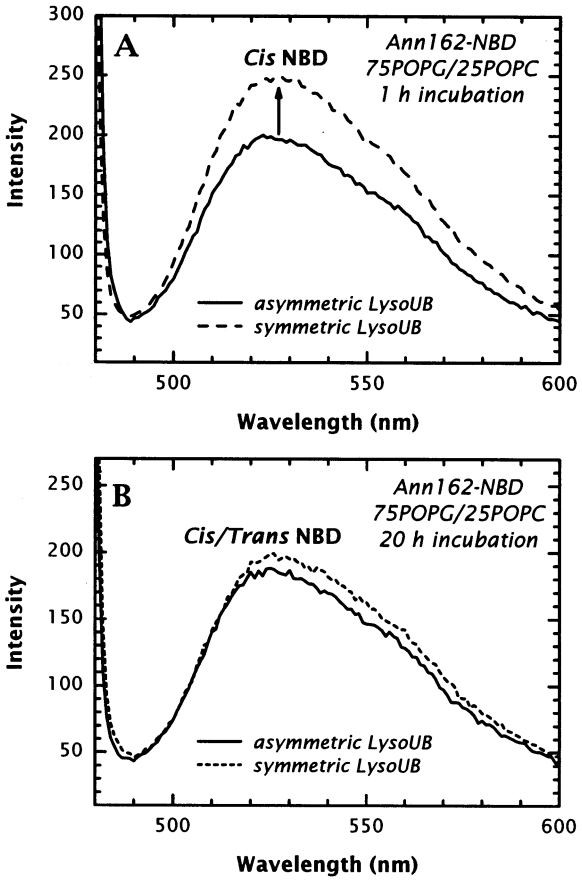

FIGURE 7: Determination of topology of the probe in Anx162-NBD inserted into 75POPG/25POPC LUV as a function of the incubation time. The samples were incubated for 1 h (A) and for 20 h (B) before the measurements. Other details are as in Figure 6. In this lipid system, unlike in the other two (see Figures 6 and 8), the probe is located in the *cis*-leaflet during the early incubation time (A). The amount of translocated probe increases with incubation to a point of nearly equal mixture of *cis* and *trans* locations (B).

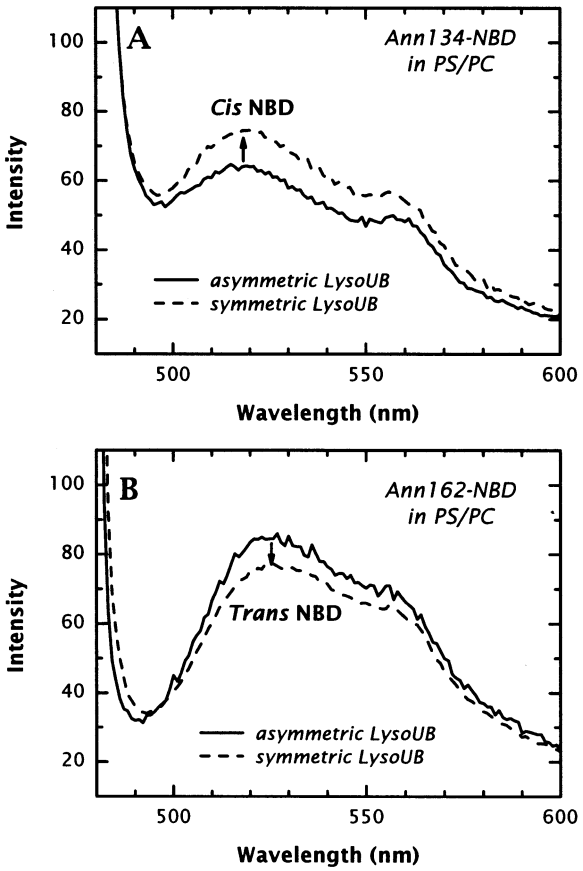

FIGURE 8: Determination of the topology of the D−E helix of annexin 12 inserted into PS/PC LUV. The samples were incubated for 5 h before the measurements. Other details are as in Figure 6. In this lipid system, the topology is the same as in 25POPC/75POPG: the probes are located in *cis*- and *trans*-leaflets for Anx134-NBD and Anx162-NBD, respectively.

step used in the earlier version of the method designed for peptides (*12*). Insertion of a protein into a membrane is a complex process involving unfolding of the aqueous structure and refolding in the membrane environment. It is conceivable that other competing events, such as aggregation of the unfolded protein, could contribute, affecting the reproducibility of the insertion. Removing the requirement for two-sample preparations thus leads to improved reliability of topology determination.

Our single-sample differential experimental scheme can, in principle, also be used with the short-range lipid quenchers. But then the effects of protein shielding, known to strongly influence quenching efficiency (*35*, *36*), must be accounted for. Our use of long-range energy transfer quenching minimizes this problem, because long-range transfer depends little on whether the donor and acceptor are separated by lipid or protein. The effects of protein shielding should thus play only a minor role when topology is determined using our method.

An important general requirement for any method that relies on asymmetric lipid distributions is that the asymmetry not be dissipated by the protein, due for example to the membrane insertion and translocation of parts of the protein. Our single-sample scheme minimizes this problem, because the quencher is added after the protein has been incorporated. If the protein were to dissipate the asymmetry completely, then no fluorescence change would be seen after alamethicin addition. A positive result (increase or decrease of intensity) is therefore observed only when (a) an asymmetric distribution of quencher exists in the presence of a protein and (b) the labeled site has a predominant cis- or trans-topology.

Water soluble quenchers are sometimes employed to determine topology. We tried using sodium dithionite to determine the topology of NBD-labeled annexin mutants, but no protection from quenching was observed under any conditions (data not shown). We suspect that the formation of a pore, or some other membrane destabilization, induced by inserted annexin (*8*) might have led to the leakage of the small water-soluble agent into the vesicles' interior, thus confusing experimental interpretation. Lipid-attached quenchers such as lysoUB, on the other hand, are unlikely to pass through such pores for two reasons. First, they form larger micelles that require larger pores to pass. And, second, because they prefer a lipid environment, even in the presence of large pores, the probability of hitting the pore precisely and going inside the vesicle without ever contacting the outer leaflet is low. As demonstrated by our model studies (Figure 4), the lysoUB method can be applied to the determination of topology of membrane-inserting proteins, such as annexins.

The annexins are a superfamily of proteins that share a common folding motif in their core domains and that bind

to the interfacial regions of membranes in the presence of Ca^{2+} at neutral pH (*32*−*34*). Under mildly acidic conditions (pH 4−5), annexin 12 refolds and forms a transmembrane structure with a water-filled pore (*8*) that mediates ion flux (*9*). The form of annexin 12 that undergoes Ca^{2+}-dependent binding to the interfacial region has the same general backbone fold as observed in the crystal structure of the protein (*19*), while the transmembrane form has a dramatically different fold (*8*). Remarkably, the transition between these two forms of the membrane-associated annexin 12 is reversible (*8*). Several bacterial toxins and colicins also undergo membrane insertion at mildly acidic pH (*1*−*7*). In neither case, however, has the process of spontaneous membrane insertion been understood on a molecular level.

To enter the membrane, annexin or any other spontaneously inserting protein must pass through the interfacial region of the bilayer, a region suggested to play an important role in protein refolding (*37*). Structurally, the interfacial region is characterized by a great degree of thermal disorder, a substantial thickness, and a high degree of chemical heterogeneity (*38*). Thermodynamically, it is characterized by a complex interplay of hydrophobic and electrostatic interactions with the polypeptide chain (*39*) and by its ability to promote secondary structure formation (*40*, *41*). On the basis of these considerations, one can reasonably assume that a posttranslational membrane protein insertion pathway should have an interfacial intermediate, one that is rich in secondary structure but lacking specific tertiary contacts of either the initial water-soluble state or the final fully inserted state. Basically, it should look like a molten globule state, only spread in the interfacial layer of the membrane, so that the lipid bilayer and the protein will constitute the hydrophobic core. [Interestingly, the molten globule state has also been suggested to play a role in translocation of water-soluble proteins (*42*, *43*).] Indeed, already identified intermediates, such as the "extended helical array" of colicin E1 channel-forming domain (*4*, *5*) or the "molten disc" of Omp A (*44*), fall into this category. If the concept is a general one, one should be able to observe a similar intermediate for annexin 12, and this intermediate should differ from a Ca^{2+}-bound interfacial state.

Our data on the kinetics and topology of the membrane insertion of NBD-labeled annexin 12 mutants are consistent with this prediction. We summarize in Figure 9 our data and those found in the literature with the schematic representation of the suggested insertion pathway for annexin 12. The D−E helix−loop−helix of repeat two of annexin 12 is highlighted on a ribbon representation of a crystallographic structure of the aqueous form (*19*). Lowering the pH ultimately results in the formation of the inserted state with the D−E region becoming a single long transmembrane helix (blue helix) and a part of a pore-forming structure (*8*). But it has not been clear which regions of the protein are forming the rest of the structure represented by gray helices. Our results (Figures 6, 8) reveal that an N-terminal part of the D−E region that includes residue 162 is translocated in the final structure. It is quite plausible that such a complex transition will have a number of discrete intermediate steps. Indeed, an insertion intermediate is clearly revealed by the biphasic kinetics of membrane interactions of Anx162-NBD with 75POPG/25POPC, because NBD fluorescence goes through a maximum at early incubation times (Figure 5A). This

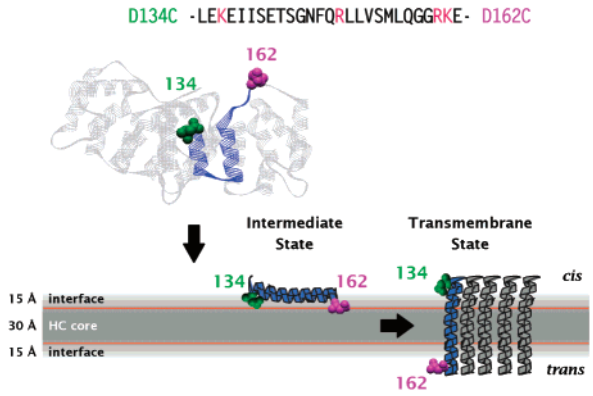

FIGURE 9: Schematic representation of the suggested insertion pathway of annexin 12. The crystallographic structure (*19*) is presented by a backbone ribbon, with the E−D helical region of repeat 2 highlighted in blue. The two aspartic acid residues shown in a CPK mode, D134 (green) and D162 (magenta), were replaced by cysteines one at a time. The mutants were labeled with NBD and the topology of Anx-134NBD and Anx162-NBD was determined in several lipid systems (Figures 6−8). In a membrane inserted state, the D−E helical region was shown to be a transmembrane helix forming a part of a water-filled pore together with not yet identified protein regions (gray helices) (*8*). Application of the novel fluorescence quenching approach described here allowed identification of the direction of the inserted region: residue 134 on the cis side and residue 162 on the trans side of the bilayer. Both fluorescence kinetics (Figure 5) and topology measurements can be rationalized by assuming the existence of an intermediate state, with an interfacial cis topology at both ends of the E−D helix. An interfacial region (highlighted by an orange line on its border with the hydrophobic core) is suggested to play a special role in the process of insertion of membrane proteins (*37*). We suggest that an interfacial intermediate is an obligatory feature of the insertion pathway. Increasing the amount of anionic lipid apparently stabilizes the interfacial intermediate state of annexin 12, perhaps due to interactions with positively charged residues (marked in red on the sequence of E−D region).

intermediate state, apparently trapped in 75POPG/25POPC, manifests itself by high intensity, as compared to 25POPG/75POPC. The rate of fluorescence change is so slow that it affords the time necessary for topology measurement, which reveals a hindered translocation in this lipid system (Figure 7). Thus, both ends of the D−E helix remain on the *cis* side of the bilayer in this intermediate state (Figure 9). Moreover, because NBD fluorescence of both labeled mutants increases immediately upon addition of LUV, the probe must be in the lipid environment when the protein is in the intermediate state. This will require a substantial unfolding of the water-soluble structure and argues for an intermediate state different from a Ca^{2+}-binding form. Indeed, no change in fluorescence of the Anx134-NBD or Anx162-NBD was observed upon mixing with LUV at neutral pH in the presence of Ca^{2+} (data not shown).

Although we do not have direct evidence that the D−E region is already a long helix in the intermediate state, we believe that this may be the case for the following reasons. The membrane interface is a strong catalyst for secondary structure formation (*41*). Consistent with this expectation, helix elongation has been reported to precede the final insertion of the colicin E1 channel domain (*4*). Another feature of colicin insertion, namely the requirement for electrostatic interactions of intermediate strength (*45*), appears to be present in annexin as well. While addition of LUV made entirely of zwitterionic POPC resulted in a

marginal change in NBD fluorescence, regardless of pH or Ca^{2+}, the insertion appears to be optimal at moderate concentration of anionic lipid and was hindered by further increase in the fraction of anionic lipid. Kinetic measurements suggest that the insertion rate decreases in the following rank order: 25POPG/75POPC (minutes) > PS/PC (hours) > 75POPG/25POPC (days). This suggests that a high fraction of anionic lipid may stabilize an interfacial form through electrostatic interactions with the cationic residues of the insertion region (marked in red on the sequence in Figure 9). The nonadditivity of electrostatic and hydrophobic interactions, demonstrated for interfacial partitioning of peptides (*39*), may also play a role in the process of membrane protein insertion and assembly. Although the lipid dependence of membrane interactions of annexin 12 requires further examination, it appears the insertion is less dependent on the specific nature of lipid headgroups or acyl chains than on the average contributions of electrostatic and hydrophobic interactions.

Fluorescence spectroscopy is a recognized tool for monitoring conformational transitions in proteins. In addition to its traditional role as a technique sensing dynamic fluctuational aspects of protein structure and its kinetic metamorphoses, fluorescence spectroscopy is increasingly assuming a new role as a direct structural tool in studies of membrane proteins (*36*, *46*). Our study reaffirms this trend by introducing a new method for determining membrane topology of proteins. It also demonstrates how the two aspects of fluorescence technique, kinetic and structural, can be combined to probe the low-resolution structure along the insertion pathway.

REFERENCES

1. Oh, K. J., Senzel, L., Collier, R. J., and Finkelstein, A. (1999) *Proc. Natl. Acad. Sci. U.S.A. 96*, 8467−8470.
2. Miller, C. J., Elliott, J. L., and Collier, R. J. (1999) *Biochemistry 38*, 10432−10441.
3. Shatursky, O., Heuck, A. P., Shepard, L. A., Rossjohn, J., Parker, M. W., Johnson, A. E., and Tweten, R. K. (1999) *Cell 99*, 293−299.
4. Zakharov, S. D., Lindberg, M., Griko, Y., Salamon, Z., Tollin, G., Prendergast, F. G., and Cramer, W. A. (1998) *Proc. Natl. Acad. Sci. U.S.A. 95*, 4282−4287.
5. Zakharov, S. D., Lindeberg, M., and Cramer, W. A. (1999) *Biochemistry 38*, 11325−11332.
6. Tory, M. C. and Merrill, A. R. (1999) *J. Biol. Chem. 274*, 24539−24549.
7. Parker, M. W., Tucker, A. D., Tsernoglou, D., and Pattus, F. (1990) *Trends Biochem. Sci. 15*, 126−129.
8. Langen, R., Isas, J. M., Hubbell, W. L., and Haigler, H. T. (1998) *Proc. Natl. Acad. Sci. U.S.A. 95*, 14060−14065.
9. Isas, J. M., Cartailler, J.-P., Sokolov, Y., Patel, D. R., Langen, R., Luecke, H., Hall, J. E., and Haigler, H. T. (2000) *Biochemistry 39*, 3015−3022.
10. Everett, J., Zlotnick, A., Tennyson, J., and Holloway, P. W. (1986) *J. Biol. Chem. 261*, 6725−6729.
11. Matsuzaki, K., Murase, O., Fujii, N., and Miyajima, K. (1995) *Biochemistry 34*, 6521−6526.
12. Wimley, W. C. and White, S. H. (2000) *Biochemistry 39*, 161−170.
13. Wimley, W. C. and White, S. H. (2000) *Biochemistry 39*, 4432−4442.
14. Haugland, R. P. (1996) *Handbook of Fluorescent Probes and Research Chemicals*, Molecular Probes, Inc., Eugene, OR.
15. Wohland, T., Friedrich, K., Hovius, R., and Vogel, H. (1999) *Biochemistry 38*, 8671−8681.
16. Shepard, L. A., Heuck, A. P., Hamman, B. D., Rossjohn, J., Parker, M. W., Ryan, K. R., Johnson, A. E., and Tweten, R. K. (1998) *Biochemistry 37*, 14563−14574.
17. Seaton, B. A. (1996) *Annexins: Molecular Structure to Cellular Function*, R. G. Landes Co., Austin.
18. Gerke, V. and Moss, S. E. (2002) *Physiol. Rev. 82*, 331−371.
19. Luecke, H., Chang, B. T., Mailliard, W. S., Schlaepfer, D. D., and Haigler, H. T. (1995) *Nature 378*, 512−515.
20. Swairjo, M. A. and Seaton, B. A. (1994) *Annu. Rev. Biophys. Biomol. Struct. 23*, 193-213.
21. Ladokhin, A.S., Isas, J.M., Haigler, H.T., & White, S.H. (2001) *Biophys. J. 80*, 539a.(Abstract)
22. Stewart, W. W. (1981) *J. Am. Chem. Soc. 103*, 7615−7620.
23. Mayer, L. D., Hope, M. J., and Cullis, P. R. (1986) *Biochim. Biophys. Acta 858*, 161−168.
24. Hope, M. J., Bally, M. B., Mayer, L. D., Janoff, A. S., and Cullis, P. R. (1986) *Chem. Phys. Lipids 40*, 89−107.
25. Moss, R. A. and Bhattacharya, S. (1995) *J. Am. Chem. Soc. 117*, 8688−8689.
26. Ladokhin, A. S., Jayasinghe, S., and White, S. H. (2000) *Anal. Biochem. 285*, 235−245.
27. Lakowicz, J. R. (1983) *Principles of Fluorescence Spectroscopy*, Plenum Press, New York.
28. Wolber, P. K. and Hudson, B. S. (1979) *Biophys. J. 28*, 197−210.
29. Davenport, L., Dale, R. E., Bisby, R. H., and Cundall, R. B. (1985) *Biochemistry 24*, 4097−4108.
30. Ladokhin, A. S., Malak, H., Johnson, M. L., Lakowicz, J. R., Wang, L., Steggles, A. W., and Holloway, P. W. (1992) In *Time-Resolved Laser Spectroscopy in Biochemistry III* (Lakowicz, J. R., Ed.) pp 562−569, SPIE, Bellingham, WA.
31. Moore, J. W., & Pearson, R. G. (1981) *Kinetics and Mechanism*, Wiley, New York.
32. Langen, R., Isas, J. M., Luecke, H., Haigler, H. T., and Hubbell, W. L. (1998) *J. Biol. Chem. 273*, 22453−22457.
33. Oling, F., Sopkova-de Oliveira Santos, J., Govorukhina, N., Mazères-Dubut, C., Bergsma-Schutter, W., Oostergetel, G., Keegstra, W., Lambert, O., Lewit-Bentley, A., and Brisson, A. (2000) *J. Mol. Biol. 304*, 561−573.
34. Reviakine, I., Bergsma-Schutter, W., Mazères-Dubut, C., Govorukhina, N., and Brisson, A. (2000) *J. Struct. Biol. 131*, 234−239.
35. Ladokhin, A. S. (1999) *Anal. Biochem. 276*, 65−71.
36. London, E. and Ladokhin, A. S. (2002) *Current Topics Membr. 52*, 89−115.
37. White, S. H., Ladokhin, A. S., Jayasinghe, S., and Hristova, K. (2001) *J. Biol. Chem. 276*, 32395−32398.
38. White, S. H. and Wiener, M. C. (1995) in *Permeability and Stability of Lipid Bilayers* (Disalvo, E. A. and Simon, S. A., Eds.) pp 1−19, CRC Press, Boca Raton.
39. Ladokhin, A. S. and White, S. H. (2001) *J. Mol. Biol. 309*, 543−552.
40. Wimley, W. C., Hristova, K., Ladokhin, A. S., Silvestro, L., Axelsen, P. H., and White, S. H. (1998) *J. Mol. Biol. 277*, 1091−1110.
41. Ladokhin, A. S. and White, S. H. (1999) *J. Mol. Biol. 285*, 1363−1369.
42. Bychkova, V. E., Pain, R. H., and Ptitsyn, O. B. (1988) *FEBS Lett. 238*, 231−234.
43. Ren, J., Kachel, K., Kim, H., Malenbaum, S. E., Collier, R. J., and London, E. (1999) *Science 284*, 955−957.
44. Kleinschmidt, J. H., den Blaauwen, T., Driessen, A. J., and Tamm, L. K. (1999) *Biochemistry 38*, 5006−5016.
45. Zakharov, S. D., Heymann, J. B., Zhang, Y.-L., and Cramer, W. A. (1996) *Biophys. J. 70*, 2774−2783.
46. Ladokhin, A. S. (2000) in *Peptides and Proteins* (Meyers, R. A., Ed.) pp 5762−5779, John Wiley & Sons, Ltd., Chichester.

BI0264418